Renewable Energy 256 (2026) 124615

Contents lists available at ScienceDirect

Renewable Energy

journal homepage: www.elsevier.com/locate/renene

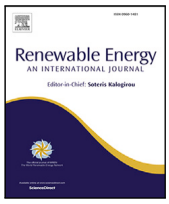

Wave energy scavenging performance of heaving and pitching ship bow foils

J.A. Bowker [a], A. Öster [b], N.C. Townsend [a,*]

[a] Faculty of Engineering and Physical Sciences, University of Southampton, UK
[b] Wärtsilä, Finland

ARTICLE INFO

Keywords:
Wave energy
Bow foils
Ship motions
Renewable energy
Energy harvesting
Energy scavenging

ABSTRACT

Bow foils have the potential to significantly improve the efficiency of marine craft. Conventionally, ship bow foils act as an energy saving device, directly converting wave energy to hydrodynamic forces, reducing the added resistance in waves and generating an additional ship thrust. In this paper, experimental results from a novel, bow foil arrangement that is free to heave relative to the ship are presented and described, as a means to generate electrical power directly. The experimental results, which demonstrate a new mode of operation for bow foils, compares the ship performance with and without the foil, on a free running 2 m bulk carrier model, over a range of wave frequencies, in regular head waves with a constant forward speed. The effect on ship motions, delivered power and the generated power, efficiency, Strouhal number and capture width ratios are presented. The results show experimentally that power can be recovered and that the system acts to reduce the pitch motion, with negligible influence on the heave motion. The concept represents a new mode of operation for bow foils and an approach for marine craft to effectively act as wave energy converters for improved efficiency and capability, with potential applications to a variety of ships that loiter e.g., patrol vessels, offshore supply vessels, wind farm crew transfer vessels and autonomous surface vehicles.

1. Introduction

1.1. Motivation

Energy scavenging, the practice of harvesting or exploiting the ambient energy for performance gains, has the potential to significantly improve the efficiency of marine craft. With the shipping industry responsible for around 940 million tonnes of CO2 annually (2.5% of worlds total CO2 emissions) and the International Maritime Organisation (IMO) legalisation requiring a shipping CO2 emissions reduction by at least 50% by 2050 compared to 2008 levels. In addition to new carbon intensity indicator (CII) energy efficiency requirements from 2023 and mandatory carbon intensity targets from 2026 [1]. Combined with the UK legally committed to reducing shipping emissions [1], becoming the first major economy in the world to legislate to reach net zero by 2050 and a signatory of the Clydebank declaration for green shipping corridors which was launched at COP26 [2]. Green maritime technologies that reduce or offset ship powering requirements and emissions is a significant and priority area. Here energy saving devices (ESDs), technologies that augment ship power or propulsion for improved efficiency, have the potential to significantly reduce carbon emissions in the shipping industry. The IMO categorises ESDs into 3 groups:

- Category A: Technologies that cannot be separated from the overall performance of a vessel.
- Category B: Technologies that can be separated from the overall performance of a vessel, operating continuously (B1) and operating intermittently dependent on the availability of an ambient energy source (B2).
- Category C: Technologies that harness energy for the reduction of auxiliary power, operating continuously (C1) and depending on the ambient environment (C2).

Following these categories, energy scavenging systems which exploit the ambient renewable energy for performance gains, for example wind propulsion technologies (WPTs) such as sails, rotors and kites (e.g., [3,4]) and wave propulsion technologies such as bow foils [5], can be categorised as B2. Whereas, energy scavenging systems which harvest the ambient renewable energy (i.e., generate electrical power) can be classified as C2.

1.2. Ship based energy scavenging systems

Various solar, wind and wave based energy harvesting systems have been proposed and studied, to improve the efficiency of marine craft.

* Corresponding author.
E-mail addresses: j.bowker@soton.ac.uk (J.A. Bowker), nick@soton.ac.uk (N.C. Townsend).

https://doi.org/10.1016/j.renene.2025.124615
Received 3 October 2024; Received in revised form 9 October 2025; Accepted 12 October 2025
Available online 16 October 2025

For example, solar (PV) energy systems have been trialled on large commercial and ocean going ships including the passenger ferry Blue Star Delos [6], the car carrier ship Auriga Leader, the hybrid car carrier Emerald Ace and a 5000 vehicle space pure car and truck carrier (PCTC) [7]. In addition, a prototype green ship in Geojeisland, South Korea [8], the MS Tûranor Planet Solar and the Kaiyu Maru [6] have all employed solar energy systems. While at the smaller scale, ocean going autonomous surface and underwater vehicles [9,10] and ocean buoys (e.g., [11,12]) regularly employ PV systems to extend mission durations. In addition to the proposed wind-augmented propulsion systems e.g. Flettner rotors, sails and kites [3,4], wind energy harvesting systems have also been proposed for direct power generation [10,13,14] and small scale commercial wind turbines (for leisure boats) are widely available.

In comparison to solar and wind, wave induced ship motion energy harvesting is still at the development stage. Sharon et al. [15] have proposed outboard heaving buoys for harvesting ship heave motions, however they provide no technical details, results or discussion of the practical implementation. Yerrapragada et al. [16] and Karami et al. [17] have proposed a 1DOF horizontal pendulum for ship motion harvesting. Similarly, Wang et al. [18] and Lu et al. [19] have proposed a vertically mounted 'eccentric disk generator' for ship motion harvesting. Mitcheson et al. [20], Toh et al. [21] and Graves et al. [22] have presented a prototype, 1DOF pendulum motion energy conversion systems for harvesting the wave-induced motions of unmanned surface vehicles (USV). Hendijanizadeh et al. [23] presented a prototype sprung moving-mass, ball screw based system for harvesting the vertical (heave) motion of a yacht. While Townsend et al. [24,25] have theoretically and experimentally investigated gyroscopic systems for harvesting the roll and pitch motions of boats and autonomous vehicles. In addition to these inertia systems, the use of submerged flapping foils for harvesting the pitching and heaving motions of autonomous surface vehicles (ASVs) has been evaluated by Bowker et al. [26] and Fenucci et al. [27], whereby the relative motions between the ASV and the submerged foils are used to generate power directly. While a concept design of a small ocean vehicle with flap-foils to harvest wave energy from the vessel roll motion is presented in [28]. Useful reviews of these wave based systems can be found in [29,30].

1.3. Paper contribution and outline

This paper proposes and experimentally investigates the performance of a novel bow foil system that is free to heave relative to the ship, to harvest the wave induced ship motion energy. The approach represents a new mode of operation, extending the performance, of bow foils.

The paper is structured as follows: Section 2 describes the experimental methodology including the experimental setup, procedures, data acquisition and control system. Section 3 presents the results of the experiments, including a comparative assessment of the effect of energy scavenging on the ship motions and delivered power, in regular head waves, with and without the foil. A discussion of the results, observations and system efficiencies are presented in Section 4 and Section 5 summarises the key insights obtained from the experimental study.

2. Experimental methodology

To evaluate the wave energy scavenging potential of heaving and pitching ship bow foils, a series of free running model tests with and without a passive, spring-loaded foil, over a range of wave frequencies, in regular head waves with a constant forward speed were conducted in the University of Southampton Boldrewood towing tank (Length = 138 m, Breadth = 6 m, Depth = 3.5 m).

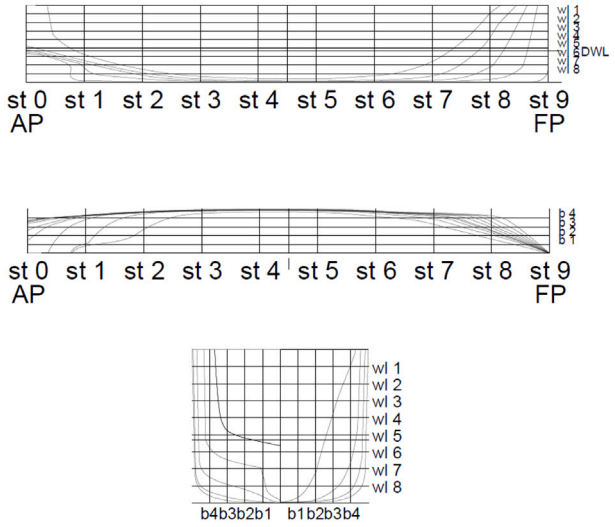

Fig. 1. Model hullform linesplan.

Table 1
Model ship particulars and nominal, 1:50 scale, full scale vessel (Representative of a small bulk carrier, block coefficient, C_b = 0.65).

Hull parameter	Model scale	Full scale
Length ($L_{oa} = L_{wl} = L_{pp}$) [m]	2	100
Breath (B) [m]	0.33	16.5
Draught (T) [m]	0.12	6
Displacement [kg, t]	51.50	6600
Vertical centre of gravity (VCG) [m]	0.14	7
Mass moment of inertia (I_{55}) [kgm^2]	12.875	4124822938
Longitudinal centre of gravity (LCG), fwd of amidships [m]	0.005	0.25

2.1. Ship model

The experiments were conducted using a free running, single screw, 2 m bulk carrier ship model. The hull linesplans are given in Fig. 1 and the model and nominal full-scale hydrostatic properties are summarised in Table 1 and presented in [5]. The model comprised of a 75 mm 4 bladed brass stock propeller (P/D = 1.025 and blade area ratio of 0.6) and a balanced (NACA0024 section) rudder.

2.1.1. Foil system

The spring-loaded foil system, illustrated in Fig. 2, consisted of a electromagnetic power take off (PTO) system (a DC motor acting as a generator) driven from the (wave induced) relative foil heave via a rack and pinion. The foil, a neutrally buoyant, rectangular uniform NACA0012 section, was 3D printed in PLA and mounted at 10% of the model length forward of the bow, such that the foil operated in the free undisturbed flow stream. The foil system and PTO parameters are summarised in Table 2.

To experimentally capture the generated electrical power the voltage across an electrical load was measured, as illustrated in Fig. 3. For a given rpm and load resistance, the load current I_L can be expressed as:

$$I_L = \frac{n}{k_n(R_{mot} + R_L)} \tag{1}$$

and the terminal voltage U_t can be measured directly or expressed as:

$$U_t = \frac{n}{k_n} - R_{mot} I_L \tag{2}$$

where n, k_n represent the generator speed (rpm), speed constant (rpm/V) and R_{mot}, R_L represent the terminal resistance (of the generator) and

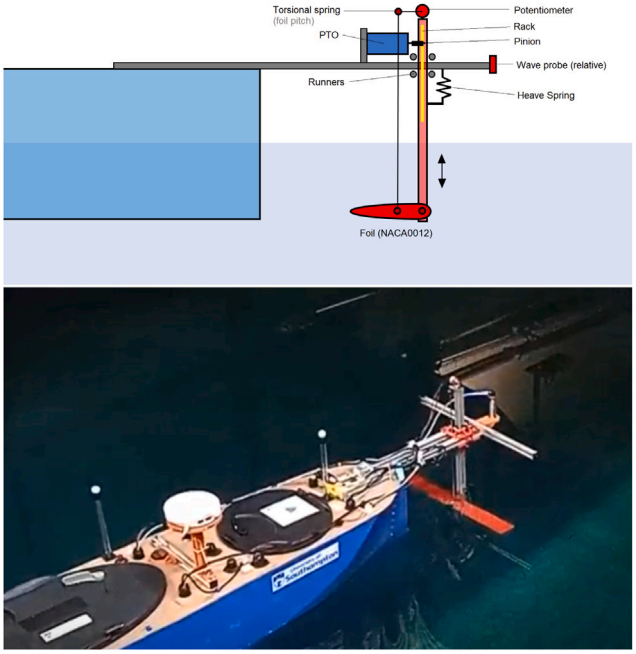

Fig. 2. Schematic (top) and photograph (bottom) of the wave energy scavenging bow foil system setup.

Table 2
Foil and PTO particulars.

Foil parameter	Details
Foil section	NACA0012
Foil span [mm]	420
Foil chord [mm]	60
Foil aspect ratio	7
Foil pitch spring constant [Nm/rad]	0.165
Foil heave spring constant [N/mm]	0.03
PTO unit (generator)	Maxon DX22S motor
PTO encoder (foil heave)	Maxon ENX16 EASY
PTO gearbox	Maxon GPX22 gearhead (6.6:1)
PTO pinion gear dia. [mm]	21
PTO speed constant [rpm/V]	1040
PTO torque constant [mNm/A]	9.18
PTO terminal resistance [Ω]	1.02
PTO load resistance [Ω]	100

load resistance respectively. Whereby, the generated electrical power is then given by:

$$P_{el} = U_t I_L \tag{3}$$

Eq. (3), a function of the measured rpm and terminal voltage, represents the electrical power output. From this, the efficiency of the generator (η_{gen}) can then be expressed as the ratio of the electrical power output (P_{el}) to the mechanical power (P_{mech}) as:

$$\eta_{gen} = \frac{P_{el}}{P_{mech}} = \frac{U_t I_L}{(K_m I_L)(\frac{2\pi}{60} n)} \tag{4}$$

where the mechanical power is given as the angular velocity multiplied by the torque ($K_m I_L$) where K_m represents the generator torque constant.

2.1.2. Data acquisition and control

The data acquisition (DAQ) and control system was based on a National Instruments myRIO1900 and Labview software. The experimental setup, based on [5] and illustrated in Fig. 5, used a local wireless network to view and control the real time Labview VI (on the model) from a laptop (host) remotely. A proportional–integral (PI) feedback controller (Fig. 4), using streamed 6DOF motions (about the longitudinal centre of gravity (LCG)) from a motion tracking camera system (Qualisys) was used to control the propeller rpm and forward speed of the model. A proportional–derivative (PD) feedback controller (Fig. 4) was used to control the rudder angle and maintain a fixed heading in the tank during each run. The sensor data, summarised in Table 3, was logged at a sample rate of 100 Hz.

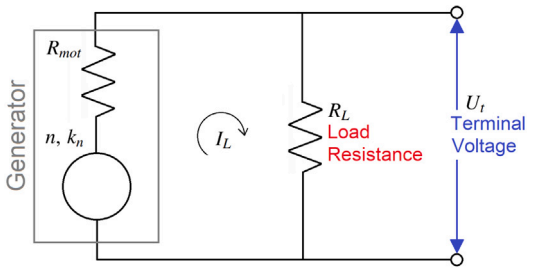

Fig. 3. Electrical circuit (of the DC motor acting as a generator).

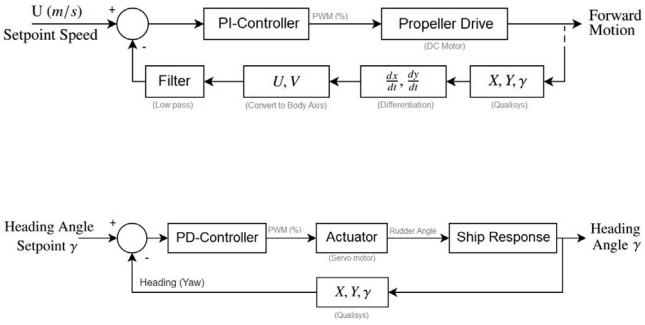

Fig. 4. Block diagram representations of the forward speed controller (top) and heading controller (bottom) (Note: to control the speed relative to the carriage, $U_{set} = 0$).

Table 3
Sensor information.

Sensor	Type	Range
Foil pitch potentiometer	Resistance	
Foil heave encoder	Digital (3 channel)	256 counts per turn
Motion capture (Qualisys)	Optical	–
Rudder potentiomenter	Resistance	±50 deg
Shaft encoder	Optical	2500 ppr
Shaft torquemeter	Full bridge	0–0.1 Nm
Wave probe (model mounted)	Ultrasonic	50–200 mm
Wave probe (carriage mounted)	Ultrasonic	

Table 4
Experimental investigations conducted with and without the foil in regular head waves (*repeated with foil x3, 'with foil only).

Parameter	Value
Wave Frequencies [Hz]	0.6', 0.7, 0.8*, 0.9, 1.0, 1.1*, 1.2, 1.3, 1.4*
Wave Amplitude [m]	0.02
Ship Model Speed [m/s]	0.5
Ship Heading [deg]	180 (head waves)
Froude Number ($V/\sqrt{gL}$)	0.1129

2.1.3. Test matrix, data handling and experimental procedure

The experimental investigations, presented in Table 4, were conducted with and without the foil system, in regular head waves, over a range of frequencies with a constant forward speed.

The conditioned model parameters are presented in Table 5. The model was conditioned prior to the experiments with an inclining test used to determine the vertical centre of gravity and shaft residual

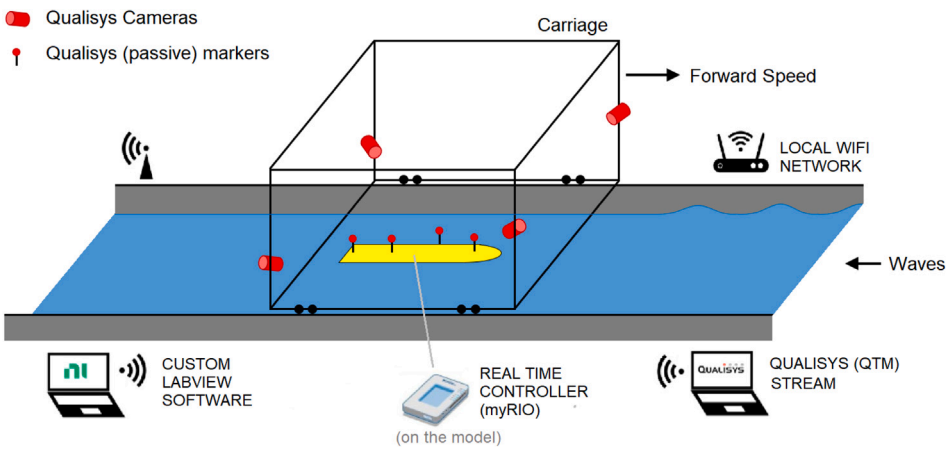

Fig. 5. Experimental Setup.

Table 5
Model conditioning.

Parameter	Measured value
Displacement[kg]	51.93
VCG [m] (measured from the keel)	0.134
Trim [deg] (bow down)	0.3
Heel [deg] (to port)	0.05
Water Temperature [°C]	17.95
Air Temperature [°C]	19.43

torque (tare) measurements were conducted before and after the experiments. Measurements of the ship motions and foil response were recorded using the onboard data acquisition system.

The experimental procedure, as illustrated in Fig. 6, comprised of an initial acceleration (carriage ramp up) (I) and constant speed in calm water (used to measure the baseline delivered power) (II), before encountering waves (III) and settling into a steady state response (IV) (with a controlled average model speed, matching the carriage speed of 0.5 m/s).

The data processing and analysis steps included:

- *Cropping:* the data was cropped into a steady-state calm-water response (Fig. 6-II) (of approximately 30 s) and a steady state wave response (of approximately 50 s) (Fig. 6-IV).
- *Filtering:* the data was filtered using a (4th order) Butterworth low-pass filter with a cutoff of 5 Hz.
- *Analysing:* the results were analysed using sine wave fitting to identify the amplitude, phase and encounter frequency.
- *Non-dimensionalise:* the results were non-dimensionalised with respect to both the frequency and magnitudes of response.

3. Results

3.1. Experimental uncertainty

To assess the repeatability (ITTC Type A uncertainty), 3 repeats at 3 wave frequencies (0.8, 1.1, 1.4 Hz) were conducted. The standard uncertainties (u), including the Student t values for a 95% confidence level following the ITTC recommendation for repeats of less than 10 [31], are summarised in Table 6. The standard uncertainty (u) and experimental standard deviations (s) of the n repeat runs were calculated as;

$$s^2 = \left(\frac{1}{n-1}\right)\sum_{k=1}^{n}(q_k - \overline{q})^2 \tag{5}$$

and

$$u = \frac{s}{\sqrt{n}} \tag{6}$$

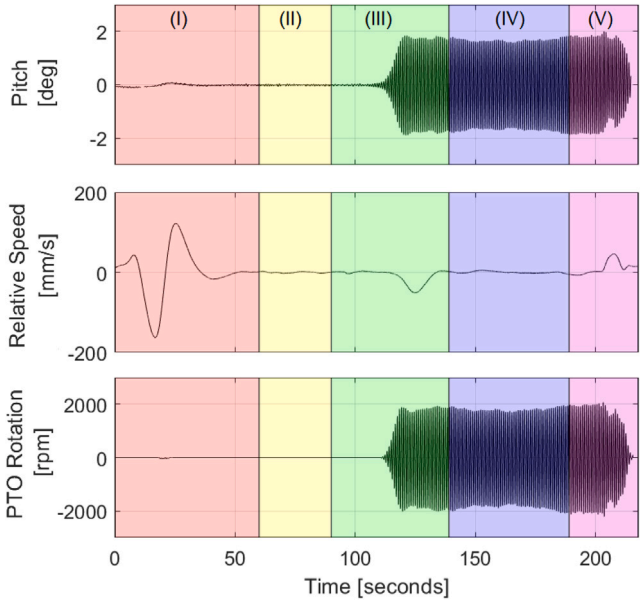

Fig. 6. Example time histories of collected data (I: Initial acceleration, II: Constant speed in calm water, III: Initial wave encounter, IV: Constant speed in waves, V: De-acceleration and end of run) ($\omega_w = 0.9$ Hz, $\zeta_a = 0.02$ m, $U_m = 0.5$ m/s).

respectively, where q represents the averaged measured values of the individual runs (calculated in calm water and encountering waves).

In addition, as summarised in Table 7, to evaluate the uncertainty of the derived metrics (delivered power, response amplitude operators (RAOs) and generated power) the expanded uncertainty (U) was calculated as;

$$U = ku_c \tag{7}$$

where k represents the coverage factor and u_c denotes the combined uncertainty, calculated (assuming variables are independent) as;

$$u_c = \sqrt{\sum_{i=1}^{N} c_i^2 u_i^2} \tag{8}$$

The sensitivity coefficients, c_i, were calculated as $\frac{\partial f}{\partial x_i}$. The results presented in Tables 6 and 7 provide a useful indication of the experimental uncertainty. The expanded uncertainties are included in the figures as error bars and the shaded bounds represent the mean expanded uncertainty.

Table 6
Standard uncertainty (u) of the measured rms values in calm water and regular waves of the repeated test runs (the Student t values ($\pm t_{95}(\frac{s}{\sqrt{n}})$) for a 95% confidence level ($t_{95} = 4.3027$) are given in brackets).

Measure	$\omega_1 = 0.8\ Hz$	$\omega_2 = 1.1\ Hz$	$\omega_3 = 1.4\ Hz$
Calmwater			
Heave [mm]	0.2088 (0.8983)	0.3488 (1.5006)	0.2581 (1.1105)
Pitch [deg]	0.0049 (0.0210)	0.0056 (0.0242)	0.0034 (0.0147)
Shaft Rev. [rpm]	3.7089 (15.9581)	1.7828 (7.6708)	3.0024 (12.9185)
Shaft Torque [mNm]	0.7598 (3.2691)	0.4071 (1.7518)	0.3210 (1.3812)
Model Speed [mm/s]	0.2098 (0.9027)	0.1545 (0.6646)	0.1305 (0.5617)
Waves			
Heave [mm]	0.1000 (0.4301)	0.0736 (0.3169)	0.0910 (0.3916)
Pitch [deg]	0.0254 (0.1094)	0.0018 (0.0079)	0.0035 (0.0150)
Shaft Rev. [rpm]	4.6574 (20.0395)	2.2183 (9.5446)	5.0342 (21.6607)
Shaft Torque [mNm]	1.2138 (5.2227)	0.2820 (1.2132)	0.8335 (3.5863)
Model Speed [mm/s]	0.6842 (2.9437)	0.3959 (1.7034)	0.9887 (4.2542)
PTO Rev. [rpm]	13.0925 (56.3329)	4.1145 (17.7033)	5.8671 (25.2445)
PTO Voltage [V]	0.0395 (0.1699)	0.0142 (0.0610)	0.0037 (0.0159)
Wave Elev. [mm]	0.1577 (0.6787)	0.1557 (0.6700)	0.1877 (0.8076)
Foil Heave [mm]	0.4622 (1.9887)	0.4284 (1.8432)	2.1493 (9.2480)
Rel. Wave (mm)	0.3419 (1.4712)	0.0606 (0.2609)	0.5745 (2.4719)

Table 7
Expanded uncertainty (U) for repeated test runs (% given in brackets) (coverage factor $k = 2$).

Measure	$\omega_1 = 0.8\ Hz$	$\omega_2 = 1.1\ Hz$	$\omega_3 = 1.4\ Hz$	Means
Delivered Power (P_{sw}) [W]	±0.089 (6.95%)	±0.047 (3.92%)	±0.039 (6.57%)	±0.059 (5.81%)
Delivered Power (P_d) [W]	±0.167 (7.62%)	±0.038 (2.19%)	±0.108 (6.57%)	±0.104 (5.46%)
Heave RAO ($\frac{z_a}{\zeta_a}$)	±0.015 (2.61%)	±0.009 (5.55%)	±0.011 (37.27%)	±0.012 (15.14%)
Pitch RAO ($\frac{z_a}{k\zeta_a}$)	±0.025 (3.17%)	±0.001 (4.91%)	±0.001 (7.73%)	±0.009 (5.27%)
Generated Power (P_{pto})	±1.329 (6.59%)	±0.091 (12.78%)	±0.022 (7.72%)	±0.481 (9.03%)
Foil Heave RAO (abs) ($\frac{h_r}{\zeta_a}$)	0.0522 (2.19%)	0.0480 (20.96%)	0.2572 (336.21%)	0.1191 (119.79%)
Foil Heave RAO (rel) ($\frac{h_r}{\zeta_r}$)	0.0252 (2.19%)	0.0011 (0.18%)	0.1474 (97.87%)	0.0579 (33.42%)

3.2. Ship motions

Fig. 7 shows the heave and pitch response amplitude operators (RAOs) with and without the energy scavenging bow-foil system. The experimental results show that the presence of the system acts to reduce the pitch motion. However, in contrast there is negligible influence on the heave motion. A pitch reduction of approximately 20% was measured at encounter frequencies of around 1 Hz (i.e. resonance).

3.3. Delivered power

The delivered power to maintain a constant speed (0.5 m/s) in calm water and when encountering regular waves, with and without the energy scavenging bow-foil system, is presented in Fig. 8. The model scale delivered power (P_d) was calculated as:

$$P_d = \frac{2\pi}{60} n(Q - Q') \tag{9}$$

from the measured shaft rpm (n) and the measured shaft torque (Q), corrected with the shaft tare (Q'), the bare torque without the propeller. As expected, the result of adding the foil system with the 20 mm aluminium strut clearly adds significant additional drag in calm water, compared to the ship without the system, and a greater total delivered power in waves. However, comparing the additional power in waves ($P_d - P_{sw}$), Fig. 8, the effect of the foil system appears to reduce the power at lower frequencies, and increase at the high frequencies compared to without the system. The reduction at lower frequencies is thought to be attributed to the reduction in pitch motion, resulting in a reduction in added resistance in waves and a delivered power saving. This finding suggests that with a hydrodynamic, low drag strut design or embodiment of the concept, the system may also be able to provide a power saving in certain conditions.

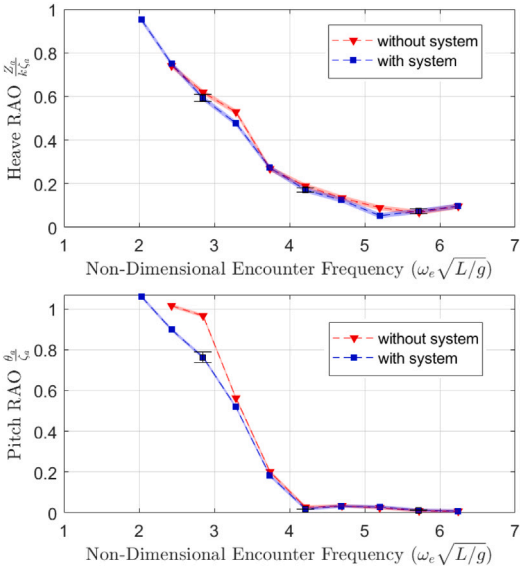

Fig. 7. Response Amplitude Operators (RAOs) with and without the energy scavenging bow-foil system (Top: Heave RAO non-dimensionalised against wave amplitude. Bottom: Pitch RAO non-dimensionlised against wave slope).

3.4. Foil motions

Fig. 9 shows the foil pitch angle responses in waves, zeroed with respect to the mean angle in the preceding calm water, constant speed section of each run prior to encountering the waves. The results, supported by observations of the experiments, show that the foil pitch response remains small throughout the tested conditions despite being passively spring loaded. For comparison, in previous bow foil studies foil pitch angles of between 10 to 20 degrees have been experimentally measured [5], albeit operating at higher forward speed (0.8 m/s compared to 0.5 m/s).

The relative foil heave response (h_r), presented as Response Amplitude Operators (RAOs) with respect to both the wave amplitude (ζ_a) and relative wave amplitude (ζ_r), are given in Fig. 10. The relative foil heave, as expected, is greatest around resonance. With respect to the wave amplitude, the measured RAO responses are relatively large (e.g., > 2). However, when considering the response with respect to the relative wave amplitude at the foil location (in effect accounting for the ship heave, pitch and the wave motion) the RAO response is found to be around 1 at lower frequencies, exhibiting a small increase towards resonance, before tailing off at higher frequencies.

3.5. Generated power

Fig. 11 shows the generator rpm and scavenged power over a range of wave frequencies. The designed system, which provides proof of concept, resulted in generator revolutions and power of up to 2000rpm and 26 mW respectively. Although, the motion response and generated power were found to exhibit a typical resonance response, it should be noted that the design of the system, including the electrical load and geared DC motor acting as a generator via the rack and pinion, may not be optimal and theoretically greater magnitudes may be possible.

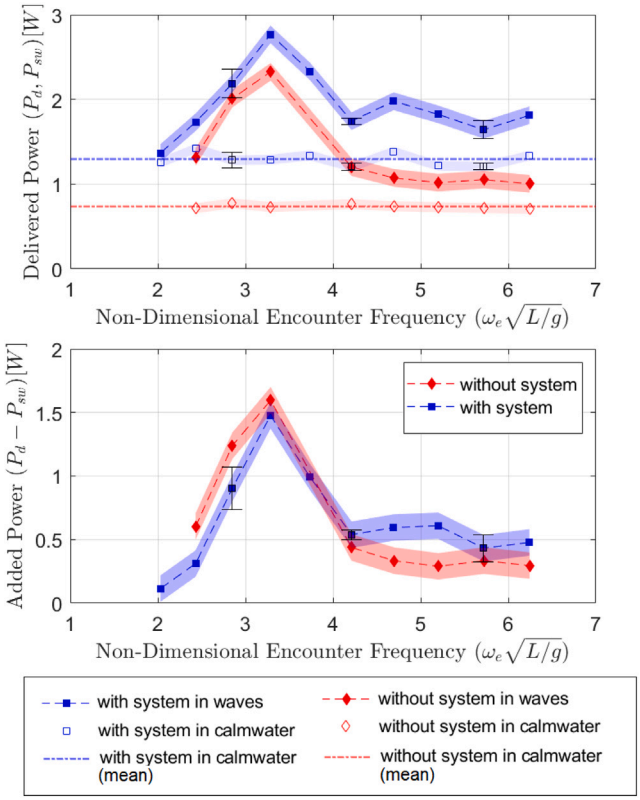

Fig. 8. Delivered power in calm-water and regular waves with and without the energy scavenging bow-foil system (Top: Delivered power, P_d, P_{sw}. Bottom: Added power in waves, $P_d - P_{sw}$).

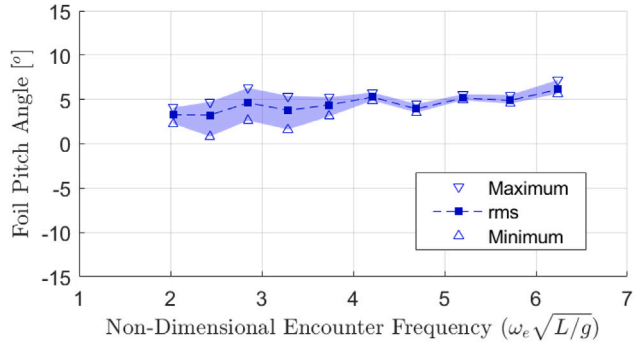

Fig. 9. Maximum, rms and minimum foil pitch angle responses in waves.

4. Discussion

4.1. System response

Experimental observations of the system response showed that the foil position remains relatively still, with the ship heave and pitch motions generating the relative motion (and power). This identified operational mode, whereby the foil system (with a greater natural frequency) largely remains unexcited, while the ship (operating around resonance) is excited, indicates that the system harvests the ship motion. In addition, the results also identified that the foil pitch angles remain small. This interesting finding is attributed to the relative heave response resulting in a reduction in the velocity over the foil, which in turn reduces the forces and moments on the foil and thus the pitch response. Practically, this indicates that changing the foil pitch stiffness

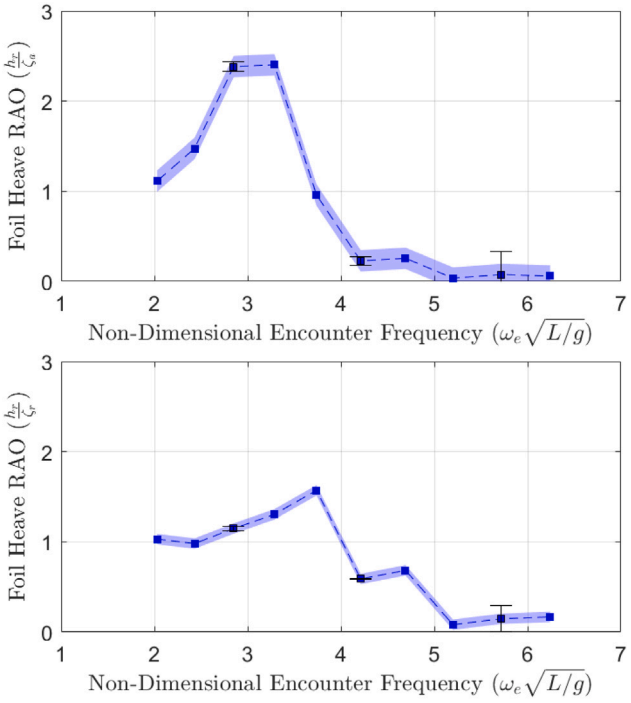

Fig. 10. The foil heave response presented as Response Amplitude Operators (RAOs) (Top: non-dimensionalised against the wave amplitude (ζ_a). Bottom: non-dimensionalised against relative wave amplitude at the bow (ζ_r)).

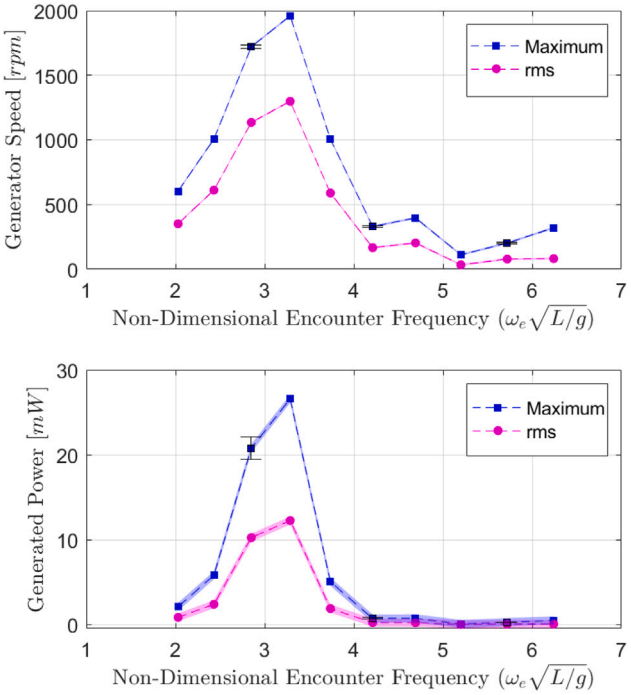

Fig. 11. Power take off (PTO) performance (Top: Generator revolutions (rpm). Bottom: Generated power (P_{gen})).

could be used to tune and further improve or control the response (e.g., thrust or power generation).

Also as the generated power, for a given PTO (k_n, R_{mot}), is a function of the rpm (n) and electrical load (R_L), there is expected to be an optimal gearing and electrical load to maximise the power (torque and

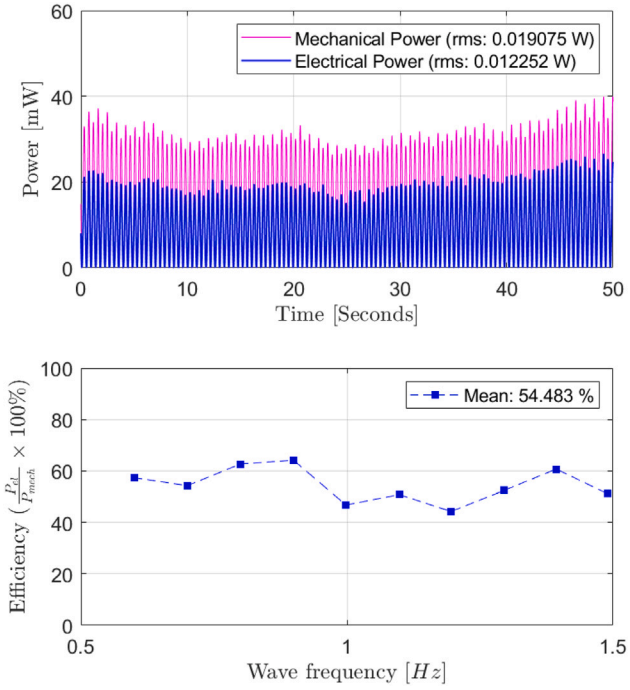

Fig. 12. Generator power and efficiency (Top: Example time history of the generated electrical and mechanical power ($\omega_w = 0.9$ Hz, $\zeta_a = 0.02$ m, $U_m = 0.5$ m/s). Bottom: Generator efficiency, η_{gen}, over the range of tested wave frequencies).

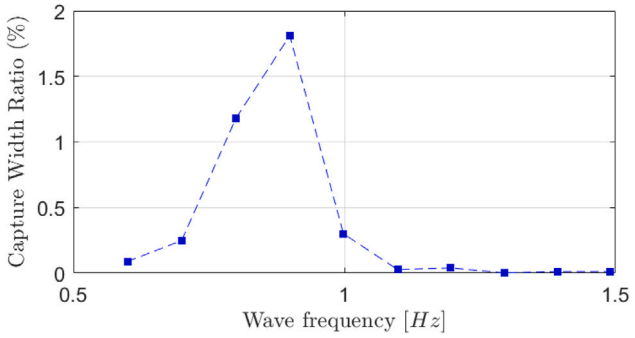

Fig. 13. Model scale capture width ratios.

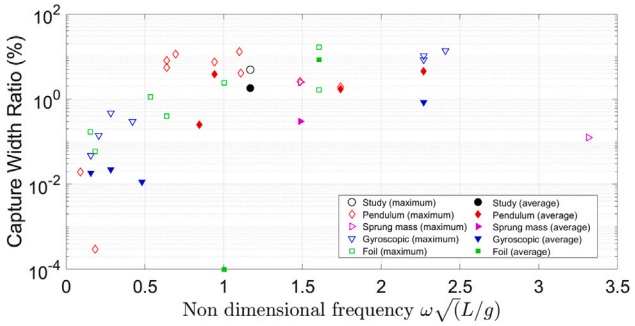

Fig. 14. Capture width ratios of prototype wave energy harvesting devices for marine buoys and autonomous systems (Calculated using reported maximum and average power assuming characteristic length, L, as either platform width (if given) or device width).
Source: [34] [22] [35] [36] [37] [38] [39] [40] [41] [42] [43] [23] [44] [45] [32] [26] [46] [27] [47] [25] [48] [49] [24] [50].

rpm), similar to theoretical studies where the PTO is often represented as a viscous damper and expressed in the form $P = \tau\omega = c\omega^2$ e.g., [25,32]. That is considering the extremes, larger damping (lower electrical load) is expected to resist and reduce the relative motion and generated power. While smaller damping (greater electrical load) is expected to reduce the torque and generated power with an optimal configuration in-between, for each condition. In this study a specific PTO setup, with fixed gearing and electric load was experimentally tested to evidence the concept. The setup may not be optimal and in practice real time control of the electrical load or gearing could lead to greater power generation, over a range of conditions.

4.2. System efficiency

Fig. 12 shows the generator efficiency (η_{gen}) (Eq. (4)), evaluated as the ratio of the electrical power output (P_{el}) to the mechanical power (P_{mech}), i.e., the motor revolutions multiplied by the torque which would be required to drive the motor at the given revolutions. The results show that the average generator efficiency is 54%, which suggests that further performance gains are achievable and that the presented power in regular waves is potentially underestimated.

A typical performance indicator for Wave Energy Converters (WECs) is the Capture Width Ratio (CWR), which can be expressed as:

$$CWR = \frac{\overline{P}_{el}}{P_w s} \times 100\% \tag{10}$$

the ratio of the average (mean) generated power ($\overline{P}_{el}$) to the wave power P_w per unit width. The $CWRs$ for the energy scavenging bow foil are presented in Fig. 13, assuming the width to be represented by the foil span, s, and the wave power is given as:

$$P_w = \frac{\rho g^2 H^2 T}{32\pi} \tag{11}$$

Experimentally, $CWRs$ of up to $\approx 1.8\%$ were achieved. Compared to model scale tests of heaving WEC devices with reported $CWRs$ of around 6%–20% [33], the results are lower. Although this is not strictly a fair comparison, with WECs designed to maximise the motions and power and ship hullforms generally designed to minimise the motions and power.

As an alternative comparison, Fig. 14 highlights the reported performance of prototype wave energy harvesting devices for marine buoys and autonomous systems. As this is an emerging research field, with various proposed mechanisms and transducers, there is a range of results. However, the comparison shows that the experimental results are encouraging, demonstrating a new mode of operation for bow foils and the similarity indicates that the concept may also be applicable to smaller scale systems such as data buoys and ASVs.

4.3. System potential

Scaling and optimisation of the system is a challenge, with the ship motions governed by Froude number, the foil forces governed by Reynolds Scaling, with variations in the environmental conditions (e.g., wave frequency, amplitude and direction), ship properties (e.g., dimensions, speed, heading), power take off design (e.g., scaling, damping and stiffness properties) and foil design (e.g., geometry, profile and stiffness). In this study, due to the dominance of gravity waves on the overall seakeeping response, Froude scaling was implemented. As a result, to provide an estimate of the full scale system performance, the model scale results were scaled following Froude scaling ($P \propto R^{3.5}$). The results, presented in Fig. 15, representing the resonance scaled power (maximum and rms values, $\omega_w = 0.9$ Hz, $\zeta_a = 0.02$ m, $U = 0.5$ m/s) provides a performance envelope, across of a range of scales, for the equivalent scaled wave amplitudes at a fixed Froude number ($F_r = 0.1129$). The results show experimentally that power can be

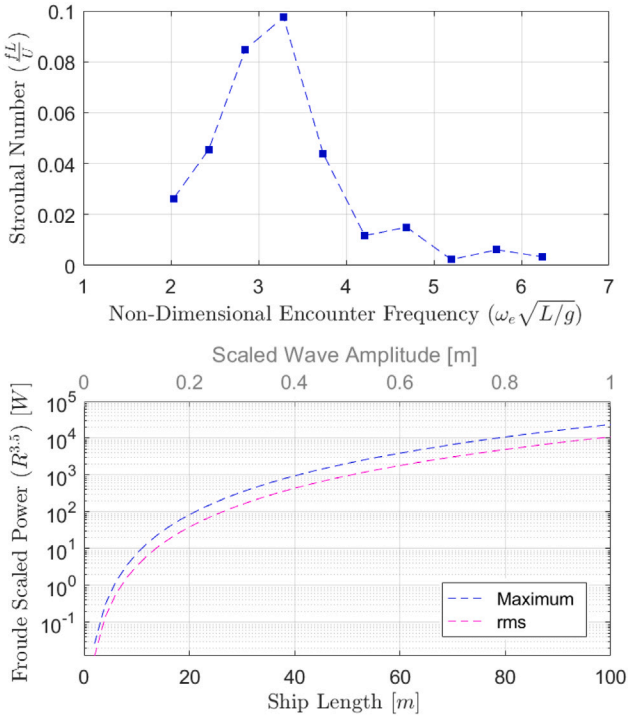

Fig. 15. Energy scavenging bow foil system performance (Top: Strouhal number, St. Bottom: Froude scaled generator power, $R^{3.5}$).

recovered, which could be used to augment on-board hotel loads and reduce emissions. While, simultaneously providing a reduction in pitch motions, increasing safety and comfort on-board which may be particularly relevant for ships that loiter e.g., patrol vessels, offshore supply vessels, wind farm crew transfer vessels and autonomous surface vehicles.

To illustrate favourable length scales and geographical locations, a global assessment based on maintaining the peak wavelength to vessel length, λ_m/L_m, to average global wavelengths, λ, was performed. The global wavelengths were calculated from the modal wave periods ($T_o = 1.41\overline{T}_z$), assuming deep water ($\lambda = \frac{g}{2\pi}T^2$), using annual, averaged wave periods (from 1993–2020) sourced from the EU Copernicus marine data store. The results, illustrated in Fig. 16 show that vessel lengths of $\approx$ 50 m, 70 m and 140 m in the Mediterranean, North Sea, and Atlantic or Pacific respectively, are favourable for the studied experimental setup. Although, caution is required in extrapolating the model-scale experimental results as the prototype is not representative of an optimised, practical, full scale system. However, the results do provide a useful indication of the performance and further research is required to identify the theoretical maximum performance and/or optimal applications.

Based on the relative heave amplitude of the foil (h_r), the encounter frequency of the ship pitch motion (f) and the ship forward speed (U), an estimate of the Strouhal number ($St = \frac{fh_r}{U}$) for the system was calculated. The results, presented in Fig. 15, identified that the system operated with Strouhal numbers of up to 0.1. In comparison, Strouhal numbers of between 0.25 and 0.35 are generally considered optimal for the propulsive efficiency of flapping foil systems. With the encounter frequency and speed related, strategies of increasing the amplitude (h_r), such as operation in relatively larger wave heights, is one approach anticipated to result in greater Strouhal numbers and potentially performance. Although an interesting observation, it should be noted that the ship parameters (U, f) that govern the Strouhal number would in practice be predefined. Furthermore, with the observations that the foil remains still, it remains to identify if the Strouhal number is a useful performance metric.

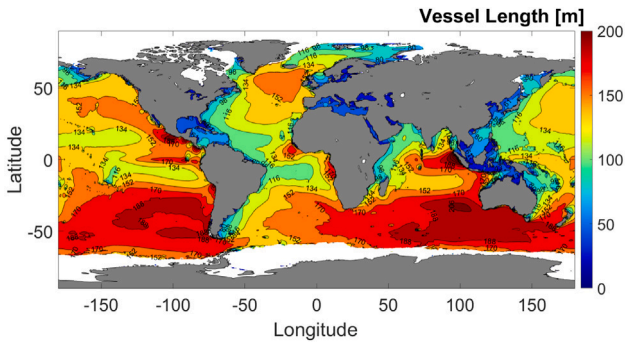

Fig. 16. Global assessment of estimated vessel lengths based on maintaining the peak wavelength to vessel length ratio (λ/L).

4.4. System improvement

While the prototype results are encouraging, providing a useful validation data-set, the tested embodiment of the concept has some notable limitations. Firstly, while the use of a strut such that the foil operates in the free undisturbed flow stream is useful for replicating the study numerically, eliminating interaction affects arising from the influence of the vessel bow wave. The strut represents a significant drag penalty and in practice a system within the hull-form with retractable foils is anticipated to be preferable from a drag and operational consideration. Secondly, the experimental system employed a passive foil. To further improve the performance, active foil control strategies are anticipated to extend the operational envelope (frequency range) and resonance response (magnitude). For example, by controlling the foil pitch angle and generating lift forces out of phase with the vertical bow motion may allow greater PTO motion and power to be generated.

5. Conclusions

This study demonstrates the feasibility of a new mode of operation for bow foils, which generates electrical power directly through the wave induced relative foil heave motion. The experimental results show that the system acts to reduce the pitch motion, by approximately 20% around resonance with negligible influence on the heave motion. Experimental observations identified that the foil position remains relatively still, with the ship heave and pitch motions generating the relative motion and power, establishing that the system harvests the ship motions. The model scale, energy scavenging bow foil system was found to generate powers of up to 26 mW, with measured generator revolutions of up to 2000rpm, operating at Strouhal numbers of up to 0.1, with Capture Width Ratios of up to 1.8%, with an average generator efficiency of 54%. The results also indicated that the additional delivered power in waves (to maintain a given speed) may be reduced at lower wave frequencies (and increased at the high wave frequencies), with the system. This finding suggests that with a hydrodynamic, low drag strut design or embodiment of the concept, the system may be able to provide a power saving in certain conditions, although further research is needed.

The proposed concept represents a new, dual mode of operation for bow foils and more widely illustrates that marine craft can effectively act as wave energy converters, for improved efficiency and capability.

CRediT authorship contribution statement

J.A. Bowker: Writing – review & editing, Software, Methodology, Investigation. **A. Öster:** Writing – review & editing, Project administration, Funding acquisition. **N.C. Townsend:** Writing – original draft, Software, Methodology, Investigation, Funding acquisition, Conceptualization.

Declaration of competing interest

The authors declare the following financial interests/personal relationships which may be considered as potential competing interests: Nicholas Townsend reports financial support was provided by European Union. If there are other authors, they declare that they have no known competing financial interests or personal relationships that could have appeared to influence the work reported in this paper.

Acknowledgment

This research was supported by the EU as part of the SeaTech project (https://seatech2020.eu/).

This project has received funding from the European Union's Horizon 2020 research and innovation programme under grant agreement No 857840

The opinions expressed in this document reflect only the author's view and in no way reflect the European Commission's opinions. The European Commission is not responsible for any use that may be made of the information it contains. This study has been conducted using E.U. Copernicus Marine Service Information;doi.org/10.48670/moi-00022

References

[1] Climate Change Committee, The Sixth Carbon Budget: The Uk's Path to Net Zero, Hydrogen Knowledge Centre, 2020.
[2] MaritimeUK, State of the maritime nation, 2022, https://www.maritimeuk.org/state-of-the-maritime-nation/.
[3] R. Lu, J.W. Ringsberg, Ship energy performance study of three wind-assisted ship propulsion technologies including a parametric study of the Flettner rotor technology, Ships Offshore Struct. 15 (3) (2020) 249–258.
[4] M. Traut, P. Gilbert, C. Walsh, A. Bows, A. Filippone, P. Stansby, R. Wood, Propulsive power contribution of a kite and a Flettner rotor on selected shipping routes, Appl. Energy 113 (2014) 362–372, http://dx.doi.org/10.1016/j.apenergy.2013.07.026.
[5] J.A. Bowker, N.C. Townsend, Evaluation of bow foils on ship delivered power in waves using model tests, Appl. Ocean Res. 123 (2022) 103148.
[6] G.M. Atkinson, Analysis of marine solar power trials on blue star delos, J. Mar. Eng. Technol. 15 (3) (2016) 115–123, http://dx.doi.org/10.1080/20464177.2016.1246907.
[7] Y. Yuan, J. Wang, X. Yan, Q. Li, T. Long, A design and experimental investigation of a large-scale solar energy/diesel generator powered hybrid ship, Energy 165 (2018) 965–978, http://dx.doi.org/10.1016/j.energy.2018.09.085.
[8] K.J. Lee, D. Shin, D.W. Yoo, H.K. Choi, H.J. Kim, Hybrid photovoltaic/diesel green ship operating in standalone and grid-connected mode–Experimental investigation, Energy 49 (2013) 475–483.
[9] D.M. Crimmins, C.T. Patty, M.A. Beliard, J. Baker, J.C. Jalbert, R.J. Komerska, S.G. Chappell, D.R. Blidberg, Long-endurance test results of the solar-powered AUV system, in: OCEANS 2006, IEEE, 2006, pp. 1–5.
[10] H.N.H. Oh, A. Tsourdos, A. Savvaris, Development of collision avoidance algorithms for the c-enduro usv, IFAC Proc. Vol. 47 (3) (2014) 12174–12181.
[11] W. Hakkarinen, Solar power on the NOMAD buoy, in: 1970 IEEE International Conference on Engineering in the Ocean Environment-Digest of Technical Papers, IEEE, 1970, pp. 240–245.
[12] A. Hegarty, G. Westbrook, D. Glynn, D. Murray, E. Omerdic, D. Toal, A low-cost remote solar energy monitoring system for a buoyed IoT ocean observation platform, in: 2019 IEEE 5th World Forum on Internet of Things (WF-IoT), IEEE, 2019, pp. 386–391.
[13] J. Kim, C. Park, Wind power generation with a parawing on ships, a proposal, Energy 35 (3) (2010) 1425–1432.
[14] J. Wellicome, A broad appraisal of the economic and technical requisites for a wind driven merchant vessel, 1975,
[15] A. Sharon, J. Briggs, H. Wirz, Mobile wave energy harvesting system, in: CleanTech2011 Conf, 2011, pp. 1–4.
[16] K. Yerrapragada, M.H. Ansari, M.A. Karami, Enhancing power generation of floating wave power generators by utilization of nonlinear roll-pitch coupling, Smart Mater. Struct. 26 (9) (2017) http://dx.doi.org/10.1088/1361-665X/aa7710.
[17] M.A. Karami, D.J. Inman, Hybrid rotary-translational energy harvester for multi-axis ambient vibrations, in: ASME 2012 Conference on Smart Materials, Adaptive Structures and Intelligent Systems, American Society of Mechanical Engineers, 2012, pp. 739–746.
[18] Y.J. Wang, Y.T. Hao, Harvesting energy from ship rolling using an eccentric disk revolving in a hula-hoop motion, in: 2014 International Power Electronics Conference, IPEC-Hiroshima - ECCE Asia 2014, 2014, pp. 1420–1424, http://dx.doi.org/10.1109/IPEC.2014.6869771.
[19] C. Lu, Y. Wang, C. Sung, P.C. Chao, A hula-hoop energy-harvesting system, IEEE Trans. Magn. 47 (10) (2011) 2395–2398.
[20] P.D. Mitcheson, T.T. Toh, K.H. Wong, S.G. Burrow, A.S. Holmes, Tuning the resonant frequency and damping of an electromagnetic energy harvester using power electronics, IEEE Trans. Circuits Syst. II: Express Briefs 58 (12) (2011) 792–796.
[21] T.T. Toh, P.D. Mitcheson, L. Dussud, S.W. Wright, A.S. Holmes, Electronic resonant frequency tuning of a marine energy harvester, in: Proceedings of the PowerMEMS, vol. 1518, Seoul, Korea, 2011, 383386.
[22] J. Graves, Y. Kuang, M. Zhu, Scalable pendulum energy harvester for unmanned surface vehicles, Sensors Actuators A: Phys. 315 (2020) 112356.
[23] M. Hendijanizadeh, S. Sharkh, M. Moshrefi-Torbati, Design guidelines for optimization of an inertially coupled energy harvesting generator from boat motion, J. Renew. Sustain. Energy 7 (4) (2015).
[24] N.C. Townsend, Self-powered autonomous underwater vehicles: results from a gyroscopic energy scavenging prototype, IET Renew. Power Gener. 10 (8) (2016) 1078–1086.
[25] N.C. Townsend, R.A. Shenoi, Feasibility study of a new energy scavenging system for an autonomous underwater vehicle, Auton. Robots 40 (6) (2016) 973–985.
[26] J. Bowker, N. Townsend, M. Tan, R. Shenoi, Experimental analysis of submerged flapping foils; implications for autonomous surface vehicles (ASVs), in: OCEANS 2016 MTS/IEEE Monterey, IEEE, 2016, pp. 1–10.
[27] D. Fenucci, A. Caffaz, R. Costanzi, E. Fontanesi, V. Manzari, L. Sani, M. Stifani, D. Tricarico, A. Turetta, A. Caiti, WAVE: A wave energy recovery module for long endurance gliders and AUVs, OCEANS 2016 MTS/IEEE Monterey, OCE 2016 (2016) 1–5, http://dx.doi.org/10.1109/OCEANS.2016.7761136.
[28] J. Zhao, T. Sun, C. Sheng, X. Yan, A concept design of a small ocean vehicle with flap-foils to harvest wave energy, in: Oceans 2016-Shanghai, IEEE, 2016, pp. 1–5.
[29] F. Zeng, T. Wang, In-situ wave energy harvesting for unmanned marine devices: A review, Ocean Eng. 285 (2023) 115376.
[30] I. McLeod, J.V. Ringwood, Powering data buoys using wave energy: a review of possibilities, J. Ocean. Eng. Mar. Energy 8 (3) (2022) 417–432.
[31] ITTC, Recommended Procedures and Guidelines: Guideline to Practical Implementation of Uncertainty Analysis, ITTC, 2021, https://www.ittc.info/media/9591/75-02-01-07.pdf.
[32] Y. Zhang, X. Han, Y. Hu, X. Chen, Z. Li, F. Gao, W. Chen, Dual-function flapping hydrofoil: Energy capture and propulsion in ocean waves, Renew. Energy 222 (2024) 119956.
[33] A. Babarit, A database of capture width ratio of wave energy converters, Renew. Energy 80 (2015) 610–628.
[34] H. Wang, T. Wang, H. Lv, S. Liu, An adjustable pendulum mechanism for in-situ wave energy harvesting in an unmanned marine vehicle, Ocean Eng. 297 (2024) 117116.
[35] P. Rui, W. Zhang, Y. Zhong, X. Wei, Y. Guo, S. Shi, Y. Liao, J. Cheng, P. Wang, High-performance cylindrical pendulum shaped triboelectric nanogenerators driven by water wave energy for full-automatic and self-powered wireless hydrological monitoring system, Nano Energy 74 (2020) 104937.
[36] H. Li, J. Lin, W. Peng, J. Jiang, T. Huang, L. Wang, Integrating a wave-excited energy harvester into an unmanned surface vehicle: Design, numerical analysis and experimental tests, Ocean Eng. 309 (2024) 118259.
[37] Y.-J. Wang, C.-K. Lee, Dynamics and power generation of wave energy converters mimicking biaxial hula-hoop motion for mooring-less buoys, Energy 183 (2019) 547–560.
[38] Y. Li, X. Ma, T. Tang, F. Zha, Z. Chen, H. Liu, L. Sun, High-efficient built-in wave energy harvesting technology: From laboratory to open ocean test, Appl. Energy 322 (2022) 119498.
[39] M. Carandell, D.M. Toma, M. Carbonell, J. del Río, M. Gasulla, Design and testing of a kinetic energy harvester embedded into an oceanic drifter, IEEE Sensors J. 20 (23) (2020) 13930–13939.
[40] W. Ding, B. Song, Z. Mao, K. Wang, Experimental investigation on an ocean kinetic energy harvester for underwater gliders, in: 2015 IEEE Energy Conversion Congress and Exposition, ECCE, IEEE, 2015, pp. 1035–1038.
[41] L. Wang, H. Li, J. Lin, X. Yan, G. Lu, S. Wu, W. Peng, Vibration energy harvesting from an unmanned surface vehicle: Concept design, open sea tests and harvester optimization, Renew. Energy 222 (2024) 119895.
[42] Y. Li, Q. Guo, M. Huang, X. Ma, Z. Chen, H. Liu, L. Sun, Study of an electromagnetic ocean wave energy harvester driven by an efficient swing body toward the self-powered ocean buoy application, IEEE Access 7 (2019) 129758–129769.
[43] C. Dai, X. Zhou, Z. Zhang, X. Wu, H. Li, P. Xu, Z. Jin, D. Li, A wave energy harvesting system based on the double-wing flywheel for unmanned surface vessels, Energy Convers. Manage. 269 (2022) 116120.
[44] D. Moreira, N. Mathias, T. Morais, Dual flapping foil system for propulsion and harnessing wave energy: A 2D parametric study for unaligned foil configurations, Ocean Eng. 215 (2020) 107875.

[45] T. Sun, J. Zhao, X. Yan, P. Xu, A new flapping-hydrofoil wave power generating unmanned ocean vehicle, in: International Conference on Offshore Mechanics and Arctic Engineering, vol. 49972, American Society of Mechanical Engineers, 2016, V006T09A016.
[46] H. Joe, H. Roh, H. Cho, S.-C. Yu, Development of a flap-type mooring-less wave energy harvesting system for sensor buoy, Energy 133 (2017) 851–863.
[47] Y. Zhang, Y. Wen, X. Han, W. Zhang, F. Gao, W. Chen, Gyroscopic wave energy converter with a self-accelerating rotor in WEC-glider, Ocean Eng. 273 (2023) 113819.
[48] Z. Pei, H. Jing, Z. Tang, Y. Fu, Experimental validation of a gyroscope wave energy converter for autonomous underwater vehicles, Appl. Sci. 11 (23) (2021) 11115.
[49] W. Chen, X. Han, Z. Liu, S. Zhou, F. Jing, R. Law, E.Q. Wu, L. Zhu, Experimental and numerical study on the performance of a gyroscopic wave energy converter under roll and pitch exciting motions, IEEE/ASME Trans. Mechatronics (2024).
[50] N. Townsend, In situ results from a new energy scavenging system for an autonomous underwater vehicle, in: OCEANS 2016 MTS/IEEE Monterey, IEEE, 2016, pp. 1–6.